15-cm Multipole Gas Ion Thruster

Gerald C. Isaacson* and Harold R. Kaufman†
Colorado State University, Fort Collins, Colo.

A 15-cm multipole thruster was operated on argon and xenon. The multipole approach used has been shown to be capable of low discharge losses and flat ion beam profiles with a minimum of redesign. This approach employs low magnetic field strengths and flat or cylindrical sheet-metal parts and hence is suited to rapid optimization and scaling. Only refractory metal cathodes were used in this investigation.

I. Introduction

THE development of electron-bombardment ion thrusters has been pursued primarily with mercury and cesium propellants. These propellants were chosen for ease of storage, ease of ionization, and high atomic weight. Researchers have demonstrated, however, that electron-bombardment thrusters can be operated on a variety of gases.[1-5] Of the cases considered in these studies, the one best suited to most space propulsion missions is xenon. The high atomic weight and ease of storage (low tankage fraction) are the major factors in this choice. Argon is a possible alternate for space propulsion if tons of propellant are required (so that cryogenic storage is practical), and excess electric power makes efficiency (and hence atomic weight) less important. Argon is also the preferred propellant in ground applications of thruster technology such as cleaning, micromachining, and ion etching of solid-state devices.

A multipole thruster was used to investigate the use of argon and xenon propellants. This thruster is related conceptually to both the multipole design of Moore[6] and Ramsey[7] and the cusped-field design of Beattie.[8] The detailed design is similar to the cusped-field thruster in that thin pole pieces of soft iron are used with electromagnets between adjacent pole pieces. The major difference from the cusped-field thruster is that more and smaller pole pieces are used, giving a larger fraction of low-field-strength volume in the ion chamber. The major similarities to the Moore and Ramsey design are the large number of pole pieces used and the general ion-chamber shape. Moore and Ramsey, however, used permanent magnets as pole pieces, with the magnetization direction toward or away from the center of the ion chamber. If permanent magnets were used in the design studied herein, they would replace the electromagnets between adjacent pole pieces rather than become the pole pieces. As an additional difference, Moore and Ramsey used much higher magnetic field strengths.

The multipole approach was used because of the general high performance level of this type. Although documented performance did not include beam profiles, past experience with a wide range of designs indicated the multipole approach should produce very uniform beams. SI (rationalized mks) units are used throughout this paper.

II. Apparatus

The 15-cm multipole thruster used in this investigation is shown in Fig. 1. This design makes extensive use of flat or cylindrical sheet-metal parts. The pole pieces are fabricated of 1.5-mm-thick "soft" iron. For the sidewalls, they are flat with an i.d. of 15 cm. The upstream pole pieces are cylindrical with mean diameters of 5, 10, and 15 cm. A center-to-center spacing of 2.7 cm was used for the pole pieces, with 1.5-mm-thick stainless-steel anodes positioned midway between each

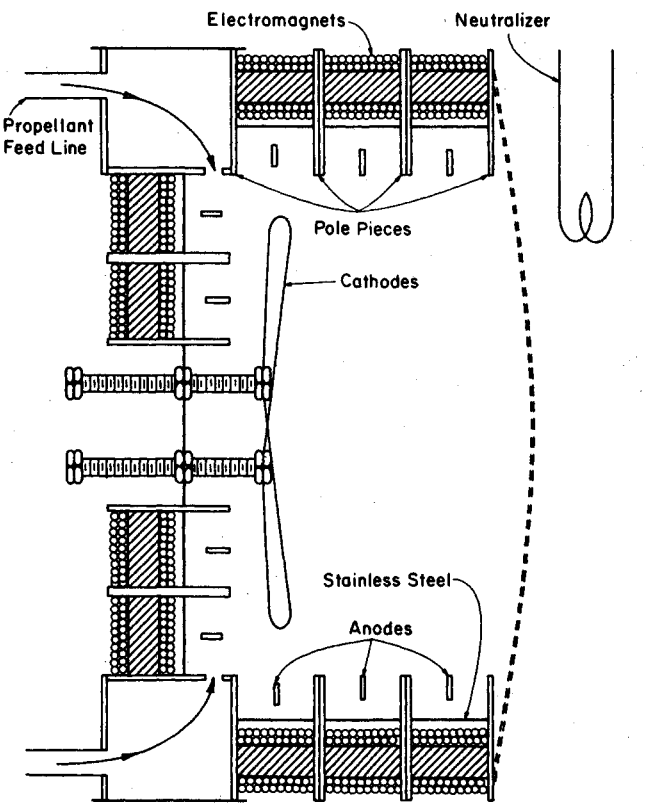

Fig. 1 Sketch of multipole gas ion thruster.

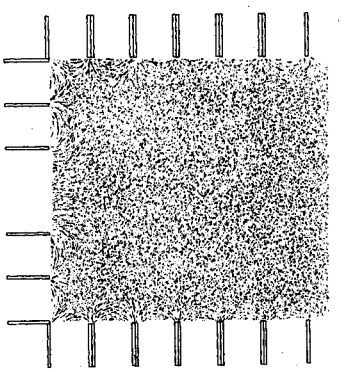

Fig. 2 Iron-filing magnetic field map.

Presented as Paper 76-1045 at the AIAA International Electric Propulsion Conference, Key Biscayne, Fla., Nov. 14-17, 1976; submitted Dec. 29, 1976; revision received March 16, 1977.

Index categories: Aerospace Technology Utilization; Research Facilities and Instrumentation; Electric and Advanced Space Propulsion.

*Research Associate. Member AIAA.

†Professor. Associate Fellow AIAA.

pair of pole pieces. Sealing of the discharge chamber was accomplished by flat stainless-steel rings located just outside the anode between each of the upstream pole pieces. Similarly, cylindrical stainless-steel pieces were used between each pair of side pole pieces. Each side section, consisting of anode, sealing ring, two pole pieces, and the electromagnets between the pole pieces, could be added or removed as a unit. This modular approach permitted the ion chamber length to be varied in 2.7-cm increments.

The magnetic configuration consisted of 12 electromagnets between each adjacent pair of side pole pieces, eight electromagnets between the 10-cm and the 15-cm diam upstream pole pieces, and four electromagnets between the 5- and the 10-cm diam upstream pole pieces. The electromagnets in each section were positioned such that each one was circumferentially midway between those in the adjoining sections. This was done to prevent any saturation problems that might occur if the electromagnets were located in line with each other. All electromagnets were connected in series, so that the current was the same through all windings. An iron-filing map of the magnetic field is shown in Fig. 2.

Dished small-hole accelerator grids (SHAG) were used with a 67% open screen and a 24% open accelerator. The thicknesses of the screen and accelerator grids were about 0.4 and 0.5 mm. The center-to-center hole spacing within a grid was about 2.2 mm, and they were assembled with an interelectrode spacing of about 1 mm. All data presented were obtained at +1000 and −500 V for screen and accelerator grid potentials.

Tungsten wire, 0.25 mm diam, was used for both the main and neutralizer cathodes. The propellant was introduced into the annular region formed by the two corner pole pieces as shown in Fig. 1. Several 6-mm holes through the pole pieces permitted flow radially inward into the ion chamber. Propellant flow was controlled with an adjustable leak valve, measured with a mass flowmeter and was maintained within ±1% of the desired value while data were being taken.

A Faraday cup probe was installed 6.5 mm downstream of the accelerator grid, which was installed convex side out. This probe was translated across the beam for current-density profiles. Details of the Faraday probe system that was used are given by Wilbur.[9] In addition, an $E \times B$ momentum analyzer was installed with the sensing probe 68 cm downstream of the accelerator grid. The probe was moveable

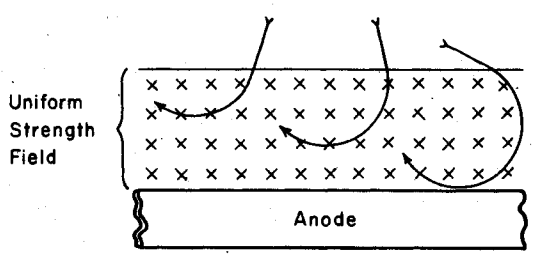

a) Simplified Deflection Configuration

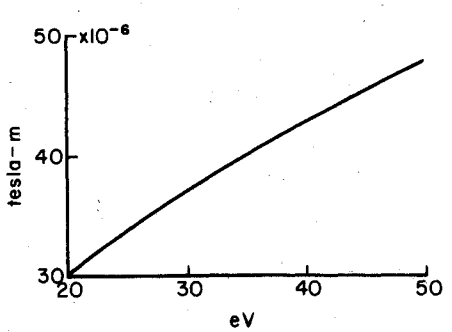

b) Required Flux per Unit Anode Length as a Function of Electron Energy

Fig. 3 Electron interaction with fringe magnetic field above anode.

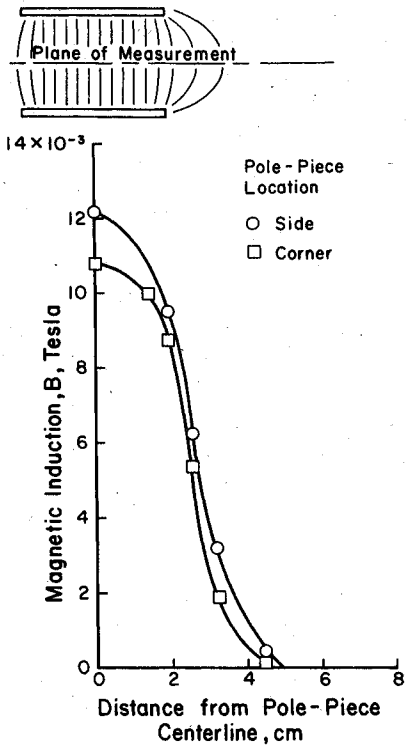

Fig. 4 Magnetic field between pole pieces.

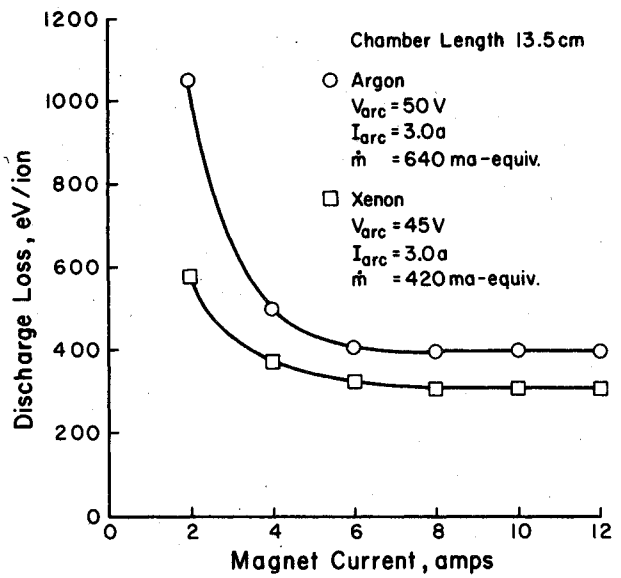

Fig. 5 Variation of discharge loss with magnet current.

transverse to the ion beam, with the path of motion passing through the center of the ion beam. Details of the sensing probe and its operation are given by Vahrenkamp,[10] with the method of analysis of the data being given by Beattie.[11] All propellant utilizations presented in this paper were corrected for double ionization and propellant backflow. The propellant backflow was calculated from facility pressure and the free-molecular-flow conductance of the accelerator system.

III. Magnetic Field

In order to determine the optimum magnetic-field strength at which to operate the thruster, a simple model was developed. This model can be illustrated with the aid of Fig. 3. The primary electrons should be contained within the ion chamber so that they expend most of their energy in producing ions before escaping to the anodes. The fringe

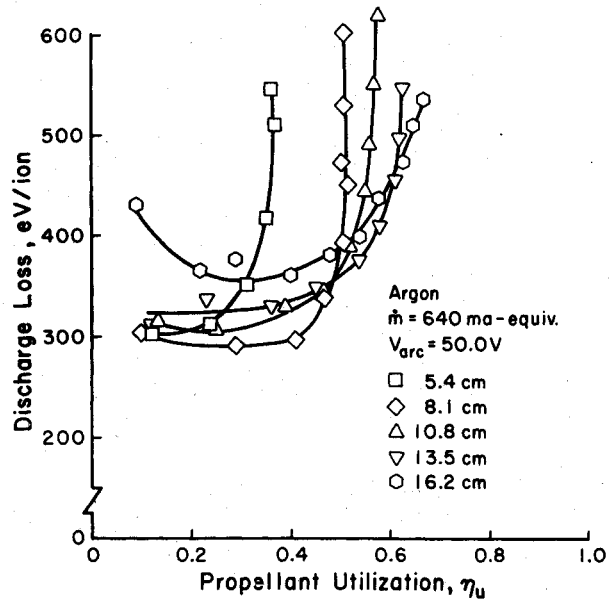

Fig. 6 Effect of chamber length on discharge-chamber performance with argon propellant.

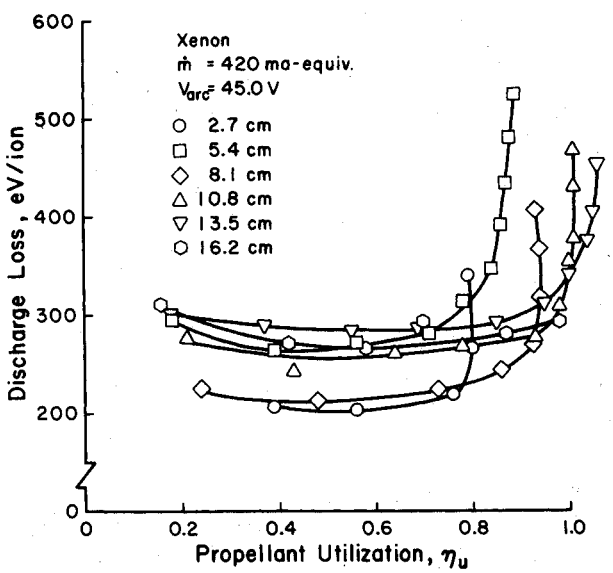

Fig. 7 Effect of chamber length on discharge-chamber performance with xenon propellant.

magnetic field between adjacent pole pieces therefore should be sufficient so that a primary electron cannot, without an intermediate collision, reach an anode. For simplicity, the fringe field is shown in Fig. 3a as a region of uniform field strength. Picking the direction of motion for a primary electron such that it has the deepest penetration into this fringe field, it is evident from Fig. 3a that this penetration corresponds to two electron cyclotron radii. The electron cyclotron radius is defined as

$$r_c = mv/eB$$

With constants evaluated, this becomes

$$r_c = 3.37 \times 10^{-6} \sqrt{eV}/B$$

This equation may be rewritten as

$$2r_c B = 6.74 \times 10^{-6} \sqrt{eV}$$

where $2r_c$ is the depth of the fringe field (above the anode) and B is the magnetic induction of this field. The product of $2r_c B$

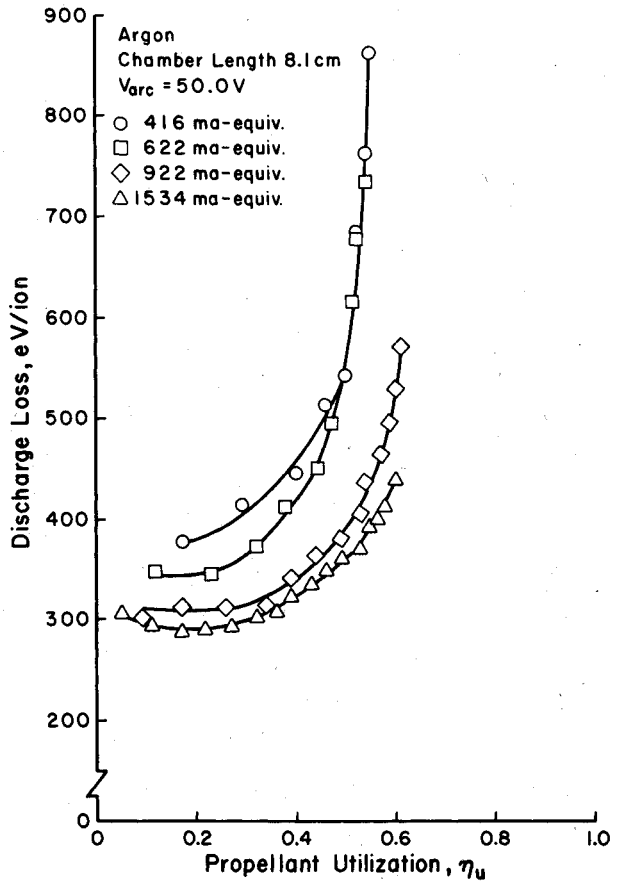

Fig. 8 Effect of flow rate on discharge-chamber performance with argon propellant.

therefore can be thought of as the flux lines per unit anode length. The distribution of these flux lines is not important. For example, half the magnetic induction extending twice as far from the anode would have the same effectiveness in deflecting primary electrons. This conclusion also was shown to be valid by Robinson and Kaufman[12] for the more realistic case of field strength varying with distance from the anode. The required flux per unit anode length is shown in Fig. 3b. For comparison of units, 50×10^{-6} T-m = 60 G-cm.

Experimental variation of the magnetic induction in the plane of the anode was obtained at various anode locations and several magnet currents. In each case, as shown in Fig. 4, the values obtained in the corner location were lower than those obtained for a side location. Integration of magnetic induction over distance normal to the anode yields the flux per unit anode length. The corner field consistently integrated to a value that was about 80% of that obtained for the side field. In order to obtain a uniform fringe field throughout the thruster, the corner anodes were recessed (behind the edges of the pole pieces) to provide the additional field. To determine the amount of recess required, the integration was carried out between the pole pieces until the field integral at the corner equalled that at the side. This was found to occur when the corner anodes were recessed by about 10% of the pole piece spacing, or 2.5 mm.

The variation of discharge loss with magnet current is shown in Fig. 5 for both argon and xenon. The discharge loss decreased with increasing magnet current for both propellants, reaching a minimum at about 8 A. Numerical integration of the fringe field at 8 A (Fig. 4) yielded about 100×10^{-6} T-m. From Fig. 3b, 45×10^{-6} T-m should have been sufficient to prevent primary electrons from reaching the anode. This factor of 2 difference between experimental performance and the theoretical model, however, is reasonable in view of the simple model used.

IV. Chamber Length

The effects of ion-chamber length on performance were investigated. The chamber length was decreased from a maximum of 16.2 cm in 2.7-cm increments for both propellants. The magnet current of 8 A was near optimum for both propellants.

Ion-chamber performance is shown in Fig. 6 for argon. Discharge losses are seen to decrease as the chamber length was decreased from 16.2 to 8.1 cm and then increased slightly with the 5.4-cm-long chamber. Operation was not possible at the 2.7-cm chamber length with argon. To obtain some insight into the trends of Fig. 6, neutral loss rates were calculated for the five chamber lengths using the method of Kaufman and Cohen[13] with a numerical value from the center of the scatter band given therein. This method gives a single neutral loss rate that should correspond to the 'knee" of the utilization vs discharge loss curve. Because the experimental scatter band is quite large, close numerical agreement should not be expected. For argon in 5.4-, 8.1-, 10.8-, 13.5-, and 16.2-cm chambers, the predicted neutral loss rates were 0.486, 0.390, 0.343, 0.315, and 0.296 A-equivalent, these neutral loss rates correspond to knee utilizations of 0.24, 0.39, 0.46, 0.51, and 0.54. These predicted knee utilizations appear to be in good agreement with the experimental values.

Similar performance data obtained for xenon are shown in Fig. 7. Again the discharge losses decrease as the chamber length was decreased from 16.2 to 8.1 cm and then increased when it was shortened further to 5.4 cm. Operation was possible at 2.7 cm with xenon and resulted in the lowest discharge losses obtained. At this length, however, the discharge was unstable and subject to extinction from any perturbation. Using the same procedure as with argon, the predicted loss rates were 0.141, 0.089, 0.071, 0.063, 0.057, and 0.054 A for chamber lengths of 2.7, 5.4, 8.1, 10.8, 13.5, and 16.2 cm. For a 0.440-A-equivalent flow rate, these neutral loss rates correspond to knee utilizations of 0.66, 0.79, 0.83, 0.85, 0.86, and 0.87. These predicted knee utilizations appear to be in reasonable agreement with the experimental values. The discrepancy between the predicted and experimental values for the three longer chambers is due at least in part to insufficient correction for double ions. Complete double-ion correction data were obtained only with the 8.1-cm-long chamber. Since the double-ion population will increase with longer chambers (note utilizations above 1.0 in Fig. 7), the use of these correction data is expected to be inadequate.

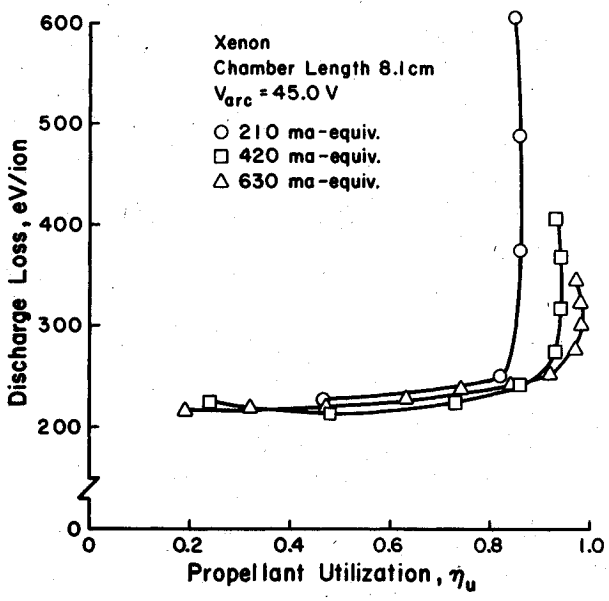

Fig. 9 Effect of flow rate on discharge-chamber performance with xenon propellant.

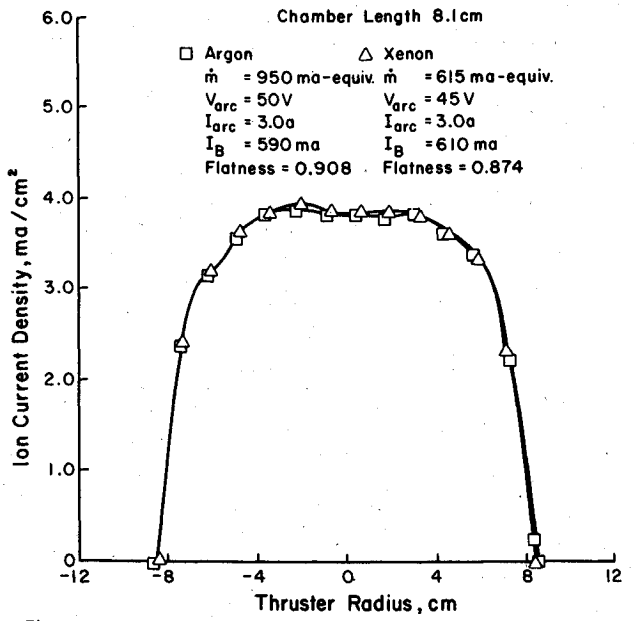

Fig. 10 Ion beam profiles for both argon and xenon propellants.

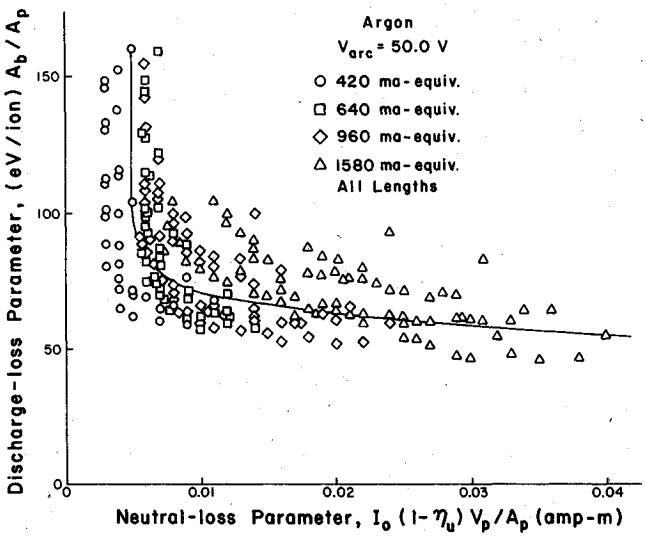

Fig. 11 Performance correlation for all discharge-chamber lengths and all flow rates with argon propellant.

V. Propellant Flow Rate

The effect of varying the propellant flow rate on thruster performance was investigated using the 8.1-cm-long chamber for both argon and xenon. Data were obtained over approximately a 3:1 range for both propellants. Data obtained with argon (Fig. 8) show minimum discharge losses of about 300 eV/ion for the 0.922- and 1.534-A-equivalent flows. The higher discharge losses for the 0.416- and 0.622-A equivalent flows are due to the neutral loss rate becoming a significant fraction (>0.5) of the neutral flow rate. Similar data obtained with xenon are presented in Fig. 9. Xenon performance is less dependent on flow, with all flows giving minimum losses of about 225 eV/ion.

VI. Ion Beam Profiles

Beam profiles were obtained in a plane 6.5 mm downstream of the center of the accelerator system. Typical beam profiles obtained with a beam current of 0.60 A for both argon and xenon are shown in Fig. 10. The profiles are quite uniform for both propellants, with flatness parameters (the ratio of average to peak current densities) at the plane of the grids of about 0.9. Based on the larger area at the survey locations,

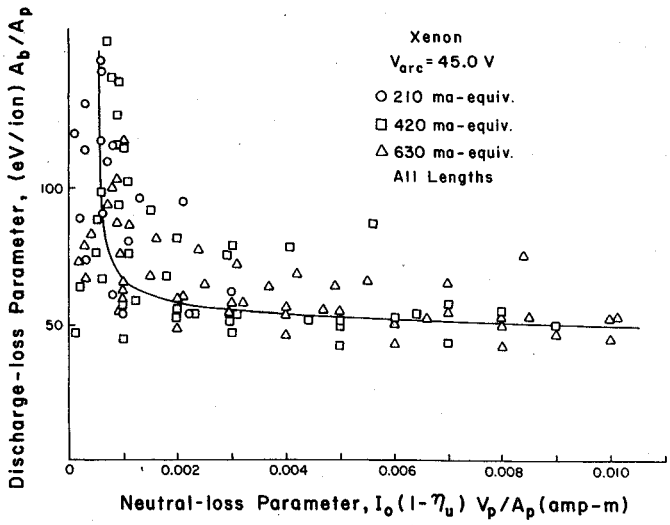

Fig. 12 Performance correlation for all discharge-chamber lengths and all flow rates with xenon propellant.

these values drop to about 0.75. The flatness parameters in the plane of the grids for all flow rates were from 0.86 to 0.93 for argon and 0.85 to 0.88 for xenon.

VII. Performance Correlation

A wider range of chamber lengths was included in this investigation than in any recent study of discharge-chamber performance. The possibility of correlating performance for different lengths therefore was examined.

The value of the neutral loss parameter, $N_0 m_i \sigma (V_p/A_p)/A_0$, in correlating "knee" performance[13] made it a promising candidate for a more general performance correlation. In the terminology of this paper, $N_0 = I_b(1-\eta_u)/\eta_u$ or $I_0(1-\eta_u)$. Using the last form, the neutral loss parameter becomes $I_0(1-\eta_u)\ m_i\sigma\ (V_p/A_p)\ /A_0$. Inasmuch as the accelerator system was constant for all data, the effective open area A_0 was omitted. Also, use of data for only one gas at a time permitted ion mass m_i and ionization cross section σ both to be omitted. These omissions left $I_0\ (1-\eta_u)\ (V_p/A_p)$, where I_0 is the total neutral flow rate in amperes, and V_p/A_p is the ratio of volume to outside area for the primary electron region. In a multipole thruster, the primary electron region can be taken as the cylindrical volume enclosed by the accelerator system and the inside edges of the pole pieces and anodes. The ratio V_p/A_p is in meters.

For a discharge-loss parameter, some means of compensating for changes in wall area (and associated wall losses) was required. The simplest approach was to multiply experimental discharge losses (electron volts per ion) by the ratio of beam area to primary electron region area, A_b/A_p. The distribution of actual losses is more complicated, but the use of this simple area ratio might be expected to give a first-order correction.

The ion-chamber data for both argon and xenon over a range of flow rates and with all chamber lengths are plotted in Figs. 11 and 12. It is evident that these parameters give a reasonable degree of data correlation for both propellants.

The expected neutral loss for the discharge-loss "knee" was calculated using the method of Kaufman and Cohen.[13] The results corresponded to neutral loss parameters of 0.0077 for argon in Fig. 11 and 0.0014 for xenon in Fig. 12. These values are in good agreement with the curves shown.

VIII. Conclusions

The multipole thruster of the type investigated herein has been shown capable of low discharge losses and flat ion-beam profiles with a minimum of optimization. Minimum discharge losses were in the range of 300-350 eV/ion for argon and 200-250 eV/ion with xenon. Flatness parameters in the plane of the grids were typically in the 0.85-0.95 range, which approaches the best values obtained previously in highly optimized designs.

The design used employs low magnetic field strengths compared to other multipole designs. Because of this low field strength and the extensive use of flat or cylindrical sheet-metal parts, the design employed is suited to rapid optimization and scaling. When this approach is exploited properly, it should be possible to translate initial performance specifications rapidly into easily fabricated, high-performance prototypes.

Acknowledgment

This work was performed under NASA Grant NSG 3011.

References

[1] Reader, P.D., "The Operation of an Electron-Bombardment Ion Source with Various Gases," NASA TM X-52006 (1964).

[2] Schertler, R.J., "Preliminary Results of the Operation of a SERT II Thruster on Argon," AIAA Paper 71-157, New York, N.Y., 1971.

[3] Byers, D.C. and Reader, P.D., "Operation of an Electron-Bombardment Ion Source using Various Gases," NASA TN D-6620, 1971.

[4] Martin, A.R., "Design and Operation of an Ion Engine using the Rare Gases," *Journal of the British Interplanetary Society*, Vol. 26, Dec. 1973, pp. 742-752.

[5] Martin, A.R., "Physical Behavior of some Biowaste Gases in an Ion Engine," AIAA Paper 73-1113, Lake Tahoe, Nev., 1973.

[6] Moore, R D., "Magneto-Electrostatically Contained Plasma Ion Thruster," AIAA Paper No. 69-260, Williamsburg, Va., 1969.

[7] Ramsey, W.D., "12-cm Magneto-Electrostatic Containment Mercury Ion Thruster Development," *Journal of Spacecraft and Rockets*, Vol. 9, 1972, pp. 318-321.

[8] Beattie, J.F., "Single Cusp Magnetic Field Thruster," *15 cm Diameter Ion Thruster Research*, edited by P.J. Wilbur, NASA Contract Rept. CR-134755, 1974, pp. 14-44.

[9] Wilbur, P.J., "Experimental Investigation of a Throttlable 15 cm Hollow Cathode Ion Thruster," NASA Contract Rept. CR-121038, 1972.

[10] Vahrenkamp, R.P., "Measurement of Double Charged Ions in the Beam of a 30 cm Mercury Bombardment Thruster," AIAA Paper 73-1057, Lake Tahoe, Nev., 1973.

[11] Beattie, J.R., "Single and Double Ion Beam Current Determination," *15 cm Mercury Ion Thruster Research—1975*, edited by P.J. Wilbur, NASA Contract Rept. CR-134905, 1975, pp. 100-106.

[12] Robinson, R.S. and Kaufman, H.R., "Application of Ion Thruster Technology to a 30-cm Multipole Sputtering Ion Source," *AIAA Journal*, Vol. 15, May 1977, pp. 702-706.

[13] Kaufman, H.R. and Cohen, A.J., "Maximum Propellant Utilization in an Electron-Bombardment Thruster," *Proceedings of the Symposium on Ion Sources and Formation Ion Beams*, Brookhaven National Lab., 1971, pp. 61-68.